Efficient Numerical approximation of Compressible Multi-material flow for unstructured meshes.

R. Abgrall$^{(*)}$, B. Nkonga$^{(*)}$ and R. Saurel$^{(\dagger)}$
($*$) Mathématiques Appliquées de Bordeaux,
33405 Talence cedex, FRANCE.
and
(†) IUSTI, Université Aix Marseille I,
13453 Marseille Cedex 13, FRANCE.

We consider the numerical approximation of multidimensional multi-material flows. This is a difficult topic related to the numerical smearing of contact discontinuities (or material interfaces or slip lines). Any Eulerian scheme will produce an artificial mixing zone. In this artificial mixture, the computation of thermodynamical variables (pressure, sound speed, temperature ..) is difficult to achieve correctly. For the stiff cases considered in this paper, with solid-liquid-gas interfaces, small errors on the thermodynamical variables lead to the blow up of the computation. In this paper, we review and explain this problem, then we propose solutions for 1D and 2D flows. Contrarily to front-tracking technics, our schemes use the same formulation everywhere on the mesh. We provide several examples with the stiffened gas equation of state (EOS) : inert materials (water-air), and chemically reactive materials (solid explosive-plexiglass-air).

1. Introduction and physical model

The computation of multi–material flows is more and more investigated because many physical situations involve interfaces and mixtures of several materials. For example, bubble–gas problems, interface problems, problems involving jets of different physical properties in rocket engines, etc. There exists a large literature about the numerical discretisation of these problems : Eulerian schemes, Lagrangian schemes, front tracking techniques [8], level set methods [6], etc. We are interested in the development of Eulerian schemes where the equation of state (EOS) is described by parameters (such as the ratio of specific heats) that may vary within the computational domain, but the analytical formulation is the same everywhere. We also want to compute flows by using the same numerical formulation everywhere and by introducing few modifications of existing conservative schemes in order to make easy the evolution of existing codes. One of our goals is to construct schemes that can be modified easily to take into account creation of species by chemical processes, or able to consider viscous phenomena. This is not possible by the Eulerian schemes using the level set formalism, for example.

In this paper, we consider gases modeled by the stiffened gas equation of state [12,11], but our technic could easily be adapted to more complex cases following for instance [26]. The stiffened gas EOS is a modification of the ideal gas EOS. It enables to consider complex situations such as compressible liquid–gas problems. More precisely, we consider problems where the pressure is related to the internal energy ϵ by

$$p = \Big(\gamma(x,t) - 1\Big)\,\rho\epsilon - \gamma(x,t)p_\infty(x,t) \tag{1}$$

where the thermodynamical parameters γ and p_∞ depend on time and space. This formulation permits to consider problems where the thermodynamical parameters are piecewise constant or even more complex situations.

"Naive" extensions of the classical conservative schemes such as Roe scheme, often lead to severe numerical problems. First, the thermodynamical parameters may reach values out of their range of validity, and second, the numerical results appear to be oscillatory and unphysical at interfaces (negative pressure, negative arguments in the computation of the sound speed). This is not a drawback of a particular scheme, but a consequence of the conservative formulation of the schemes [1–4,14]

Many investigations have been done to define an efficient numerical approximation for multi-material flows, see for example [1,15], and [3] for a review. Most of the time, these oscillations are barely visible, but in some cases (large pressure or density ratio at interfaces, very different EOS), they can lead to the blow up of the computation. Therefore, the major challenge is the numerical characterization of the material properties, in the mixing zone and the handling of pressure oscillations across material interfaces.

The previous investigations done in this topic are always based on 1-D analysis or in several dimensions but for very regular meshes [24]. In this basically 1D techniques, the system of PDEs is discretised in such a way that the mass, momentum and total energy are locally conserved, hence the correct shock speed can be computed. The flow composition is updated such that, in the case of a perfect contact discontinuity, the velocity and the pressure remain uniform. However, this method cannot be easily generalized to several dimensions, especially when the mesh is unstructured or very distorted structured mesh, because there are no natural direction in the mesh.

In this paper, we show how to extend the method of [2,24] to general unstructured meshes. A careful analysis is conducted and enables to alleviate the remaining difficulties contained in [2] about high order extensions, and to proceed the multidimensional case easily. More precisely, we first discuss our model, then consider the continuous case to illustrate the general principles of the paper. The one–dimensional discrete case is then illustrated by the Roe, Godunov and Rusanov schemes, with a particular emphasis on the Roe scheme. Then, we discuss the multidimensional case, and show which additional modifications have to be made to take properly into account the physics of slip lines. We conclude by showing how the method can be used for flows with chemistry, and different test cases are discussed.

2. The physical model

We consider a flow which dynamic is governed by the compressible Euler equations. In this context, the conservative formulation of the multi-fluid flow reads:

$$\left\{\begin{array}{lclcl} \partial_t\rho & + & \nabla\cdot(\rho\boldsymbol{u}) & & = 0\\ \partial_t\boldsymbol{m} & + & \nabla\cdot(\boldsymbol{m}\otimes\boldsymbol{u}) & + \nabla p & = 0\\ \partial_t E & + & \nabla\cdot(\rho H\boldsymbol{u}) & & = 0\end{array}\right. \tag{2}$$

where ρ is the density, $\boldsymbol{u}$ the velocity, $\boldsymbol{m} = \rho\boldsymbol{u}$ the momentum, E the total energy, p the hydrodynamic pressure and $H = (E+p)/\rho$ the specific enthalpy. This system is generally written in the following form:

$$\partial_t W + \mathrm{div}\,(\boldsymbol{F}) = 0$$

The pressure is related to the other variables by the equation of state (1). For simplicity reasons, we rewrite the "stiffened" gas EOS as:

$$\beta p + \theta = E - \frac{1}{2}\rho\boldsymbol{u}\cdot\boldsymbol{u}$$

where

$$\beta := \frac{1}{\gamma - 1} \ \text{ and } \ \theta := \frac{\gamma p_\infty}{\gamma - 1}$$

are the thermodynamical parameters. Their evolutions are governed by the equations:

$$\partial_t\beta \ + \ \boldsymbol{u}\cdot\nabla\beta \ = \ 0, \qquad \text{and} \qquad \partial_t\theta \ + \ \boldsymbol{u}\cdot\nabla\theta \ = \ 0. \tag{3}$$

We note that an equivalent conservative form of the equations can be written,

$$\begin{array}{l}
\partial_t\rho + \nabla\left(\rho\boldsymbol{u}\right) = 0\\
\partial_t\left(\rho\boldsymbol{u}\right) + \nabla\left(\rho\boldsymbol{u}\otimes\boldsymbol{u}\right) + \nabla p = 0\\
\partial_t E + \nabla\left(\rho H\boldsymbol{u}\right) = 0\\
\partial_t\left(\rho\beta\right) + \nabla\left(\rho\beta\boldsymbol{u}\right) = 0\\
\partial_t\left(\rho\theta\right) + \nabla\left(\rho\theta\boldsymbol{u}\right) = 0.
\end{array} \tag{4}$$

Other equivalent systems could be obtained. We rely on this particular form to explain our technic, even though the other systems might also have been considered instead.

The system (2,3) or (4) is hyperbolic. In the 1D case, the eigenvalues are u, $u - c$ and $u + c$ where the sound speed is defined by

$$c^2 = \frac{\gamma(p + p_\infty)}{\rho}$$

Across a contact discontinuity, the pressure and the velocity remain constant. In the multidimensional case, it is the pressure and the normal velocity.

3. Numerical Model: 1-D Case

3.1. General principles

We begin with a description of the governing principles of our technique on system (2) in 1D. Consider $\Delta x > 0$, $x_i = i\Delta x$ for $i \in \mathbb{Z}$, $\delta t > 0$ and the conservative scheme

$$\begin{array}{lcrcl}
\delta\rho & + & \nu\Delta F_\rho & = & 0\\
\delta\rho u & + & \nu\Delta F_{\rho u} & = & 0\\
\delta E & + & \nu\Delta F_E & = & 0.
\end{array} \tag{5}$$

In (5), we make use of the notation, for any function f, $\delta f := f^{n+1} - f^n$, $\Delta f := f_{i+1/2} - f_{i-1/2}$ and $\nu = \frac{\delta t}{\Delta x}$.

The question is to find a discretisation of the non–conservative system (3) compatible with the physics of (2–3), namely the velocity and the pressure should stay continuous across material interfaces. It is well known that the smooth solutions of (2) are solutions of

$$\partial_t \rho + u\partial_x \rho + \rho \partial_x u = 0 \tag{6}$$
$$\rho \partial_t u + \rho u \partial_x u + \partial_x p = 0 \tag{7}$$
$$\partial_t p + u\partial_x p + \rho c^2 \partial_x u = 0. \tag{8}$$

The last equation is equivalent to the transport of physical entropy. The system (6-7-8) can be obtained from (2–3) by algebraic manipulations. The first equation is obtained by developing $\partial_t \rho + \partial_x \rho u$. The second one is

$$-u\left(\partial_t \rho + \partial_x \rho u\right) + \Big(\partial_t \rho u + \partial_x \rho u^2 + \partial_x p\Big) = 0,$$

and the last one is obtained in two steps :

- First

$$\begin{aligned} \partial_t \rho\epsilon + u\partial_x \rho\epsilon + p\partial_x u &= \Big(\partial_t E + \partial_x [u(E+p)]\Big) \\ &- u\Big(\partial_t \rho u + \partial_x \rho u^2 + \partial_x p\Big) + \frac{u^2}{2}\Big(\partial_t \rho + \partial_x \rho u\Big) \end{aligned}$$

- second, since $\rho\epsilon = \beta p + \theta$,

$$\begin{aligned} \partial_t \rho\epsilon + u\partial_x \rho\epsilon + p\partial_x u &= p\Big(\partial_t \beta + u\partial_x \beta\Big) \\ &+ \Big(\partial_t \theta + u\partial_x \theta\Big) + \beta\Big(\partial_t p + u\partial_x p + \rho c^2 \partial_x u\Big) \end{aligned}$$

Our technique is to mimic these algebraic manipulations and to identify discrete operators that are consistent with the continuous operators between the brackets above.

We have $\delta E = \delta(\rho\epsilon) + \frac{1}{2}\delta(\rho u^2)$. The idea is to write a scheme for the internal energy by combining the equations for E, ρu and ρ. For an *explicit scheme*,

$$\begin{aligned} \delta\big(\rho u^2\big) &= (\rho u)^{n+1}\delta u + u^n \delta\rho u \\ \\ \delta\big(\rho u\big) &= \rho^{n+1}\delta u + u^n \delta\rho \end{aligned} \tag{9}$$

and then,

$$\delta(\rho\epsilon) = \delta E - \frac{u^n + u^{n+1}}{2}\delta\rho u + \frac{u^n u^{n+1}}{2}\delta\rho \tag{10}$$

that is

$$\delta(\beta p+\theta)+\nu\left(\Delta F_E-\frac{u^n+u^{n+1}}{2}\Delta F_{\rho u}+\frac{u^n u^{n+1}}{2}\Delta F_\rho\right)=0. \tag{11}$$

We rewrite the flux variation of any Q-scheme [9], $\Delta F=F_{j+1/2}-F_{j-1/2}$ as

$$\begin{aligned}\Delta F &= F_{j+1/2}-F_{j-1/2}\\ &= \tfrac{1}{2}\left(\Psi_{j+1/2}+\Psi_{j-1/2}\right)\end{aligned}$$

where $\Psi_{j+1/2}=(F_{j+1}-F_j-Q(W_{j+1}-W_j))$. In the sequel, we often call $\Psi_{j+1/2}$ a fluctuation, and call

$$\Delta F=\frac{1}{2}\left(\Psi_{j+1/2}+\Psi_{j-1/2}\right)$$

the fluctuation form of the scheme

Denoting by ℓ_j the vector $\ell_j=(\frac{u_j^n u_j^{n+1}}{2},-\frac{u_j^n+u_j^{n+1}}{2},1)^T$, equation (11) can be rewritten as $\delta(\beta p+\theta)=\delta(\beta p+\theta)_{j+1/2}+\delta(\beta p+\theta)_{j-1/2}$ where

$$\delta(\beta p+\theta)_{j+1/2}=\frac{1}{2}\ell_j\ .\ (\Psi_\rho,\Psi_{\rho u},\Psi_E)^T_{j+1/2}$$

$$\delta(\beta p+\theta)_{j-1/2}=\frac{1}{2}\ell_j\ .\ (\Psi_\rho,\Psi_{\rho u},\Psi_E)^T_{j-1/2}$$

Then, we can rewrite, for *an explicit scheme*, $\delta(\beta p+\theta)_{j+1/2}$ as

$$\delta(\beta p+\theta)_{j+1/2}=\left(p_j^n\delta\beta_{j+1/2}+\delta\theta_{j+1/2}\right)+\beta_j^{n+1}\delta p_{j+1/2}.$$

The last step is to identify in $\frac{1}{2}\ell_j\ .\ (\Psi_\rho,\Psi_{\rho u},\Psi_E)^T_{j+1/2}$ the terms that are consistent with $\beta_j^{n+1}\delta p_{j+1/2}$, $p_j^n\delta\beta_{j+1/2}$ and $\delta\theta_{j+1/2}$ in the limit of a mesh refinement. A guide is that the evolution scheme for p should preserve the pressure in the case of a contact discontinuity, as in [2,23]. In the following, we illustrate this technique for Roe's, Godunov's and Rusanov's schemes and for a second order MUSCL type scheme.

Remark 3.1. *For an implicit scheme, we would have switched the superscript $n+1$ and n in (9) and made the modification accordingly in (10).*

3.2. Case of Roe's scheme

For Roe's scheme [19], $Q_{j+1/2}=|\mathcal{J}(W_j,W_{j+1})|$ and the calculations can be carried out easily.

We first recall some basic facts about Roe's scheme. The average Jacobian matrix $\mathcal{J}(W_j,W_{j+1})$ satisfies the jump condition

$$F(W_{i+1})-F(W_i)=\mathcal{J}(W_j,W_{j+1})\ (W_{i+1}-W_i)\,.$$

The Jacobian A of the flux F depends on the velocity u, the total enthalpy H and additional parameters, namely the derivative of the pressure with respect to the density and the internal energy, p_ρ, p_ϵ.

To obtain an average Jacobian matrix that reduces to the standard one for a perfect gas, it is usefull to note that it should depend on the Roe average of the velocity, the Roe average of the total enthalpy, and the following jump relation should be satisfied,

$$\Delta_{j+1/2}p = \widetilde{p_\rho}\Delta_{j+1/2}\rho + \widetilde{p_m}\Delta_{j+1/2}m + \widetilde{p_E}\Delta_{j+1/2}E + \widetilde{p_{\rho\beta}}\Delta_{j+1/2}\left(\rho\beta\right) + \widetilde{p_{\rho\theta}}\Delta_{j+1/2}\left(\rho\theta\right) \tag{12}$$

There are many possible choice for $\widetilde{p_\rho}$, $\widetilde{p_\epsilon}$, etc. What is important is that at the end, the characteristic decomposition of $\Delta_{j+1/2}W := W_{j+1} - W_j$, in terms of the eigenvectors of $\mathcal{J}(W_j, W_{j+1})$, is very simple. The calculations are given in Appendix A, as well as all the components of the averaged matrix and the right and left eigenvectors.

Let us characterize the upwinding process by a function φ (for the Roe scheme $\varphi(u) = |u|$). Setting $\varphi^{\pm}(X) = \frac{X\pm\varphi(X)}{2}$, equation (10) can be written explicitly as

$$\begin{aligned}\delta\beta p_{j+1/2} + \delta\theta &= -\mathcal{A}\varphi^-(\bar{u})\left(\Delta_{j+1/2}\rho - \tfrac{\Delta_{j+1/2}p}{\bar{c}^2}\right) - \mathcal{B}\frac{\Delta_{j+1/2}p}{\bar{c}^2} - \mathcal{C}\underline{\rho}\frac{\Delta_{j+1/2}u}{\bar{c}} + \mathcal{D}\\ &\quad -\nu\varphi^-(\bar{u})p_i\Delta_{j+1/2}\beta - \nu\varphi^-(\bar{u})\Delta_{j+1/2}\theta\end{aligned} \tag{13}$$

with $\widetilde{u}_{j+1/2} = \frac{u_j^n + u_j^{n+1}}{2}$, $\widetilde{q}_{j+1/2} = \frac{u_j^n u_j^{n+1}}{2}$, $\mathcal{A} = \nu(\bar{u}^2 - 2\bar{u}\widetilde{u}_{j+1/2} + 2\widetilde{q}_{j+1/2})$, $\underline{\rho} = \sqrt{\rho_j\rho_{j+1}}$,

$$\begin{aligned}2\mathcal{B} &= \nu\varphi^-((\bar{u}+\bar{c}))\left((\bar{H}+\bar{u}\bar{c}) - \widetilde{u}_{j+1/2}(\bar{u}+\bar{c}) + \widetilde{q}_{j+1/2}\right)\\ &+ \nu\varphi^-((\bar{u}-\bar{c}))\left((\bar{H}-\bar{u}\bar{c}) - \widetilde{u}_{j+1/2}(\bar{u}-\bar{c}) + \widetilde{q}_{j+1/2}\right)\\ \mathcal{D} &= \nu\varphi^-(\bar{u})(\underline{p} - p_i)\Delta_{j+1/2}\beta.\end{aligned}$$

and

$$\begin{aligned}2\mathcal{C} &= \nu\varphi^-((\bar{u}+\bar{c}))\left((\bar{H}+\bar{u}\bar{c}) - \widetilde{u}_{j+1/2}(\bar{u}+\bar{c}) + \widetilde{q}_{j+1/2}\right)\\ &- \nu\varphi^-((\bar{u}-\bar{c}))\left((\bar{H}-\bar{u}\bar{c}) - \widetilde{u}_{j+1/2}(\bar{u}-\bar{c}) + \widetilde{q}_{j+1/2}\right).\end{aligned}$$

The terms $\mathcal{A}\bar{u}^+\left(\Delta_{j+1/2}\rho - \frac{\Delta_{j+1/2}p}{\bar{c}^2}\right) + \mathcal{B}\frac{\Delta_{j+1/2}p}{\bar{c}^2} + \mathcal{C}\underline{\rho}\frac{\Delta_{j+1/2}u}{\bar{c}} + \mathcal{D}$ are consistent with $up_x + \rho c^2 u_x$, i.e. in the limit of a mesh refinement, and for smooth solution, we get $up_x + \rho c^2 u_x$. The identification we have performed here is choosen in order to prevent the instabilities of p and $\boldsymbol{u}$ that can occur in 2D computations when the pressure is not uniform.

We can write $\delta(\beta p)_j = \beta_j^{n+1}\delta p + p_j^n \delta\beta$, and a natural discretization is thus

$$
\begin{array}{rcl}
\delta\beta_{j+1/2} &=& -\nu\varphi^-(\bar{u}_{j+1/2})\Delta_{j+1/2}\beta \\
\delta\theta_{j+1/2} &=& -\nu\varphi^-(\bar{u}_{j+1/2})\Delta_{j+1/2}\theta \\
\\
\delta\beta_{j-1/2} &=& -\nu\varphi^+(\bar{u}_{j-1/2})\Delta_{j-1/2}\beta \\
\delta\theta_{j-1/2} &=& -\nu\varphi^+(\bar{u}_{j-1/2})\Delta_{j-1/2}\theta
\end{array}
\tag{14}
$$

and

$$
\begin{array}{rcl}
\delta\beta_j &=& \delta\beta_{j+1/2} + \delta\beta_{j-1/2} \\
\delta\theta_j &=& \delta\theta_{j+1/2} + \delta\theta_{j-1/2},
\end{array}
$$

where, $\varphi^-(\bar{u}) = \bar{u}^-$ and $\varphi^+(\bar{u}) = \bar{u}^+$ for the Roe scheme. It clearly prevents oscillations in the pressure (the contacts are perfectly described). It also admits a maximum principle on β and θ under the CFL like condition

$$\nu \max_j \left(\varphi^-(\bar{u}_{j+1/2})\right) \leq 1.$$

The conservation of the density, momentum and total energy is guaranteed.

3.3. Case of Godunov scheme

Consider $\mathcal{F}(W_j, W_{j+1}) = F(W^*_{j+1/2})$ the flux for Godunov scheme [10] for (4) between the left and right states W_j and W_{j+1}, see Figure 1. As we have seen above, the important quantities are not the flux but the residuals

$$
\left\{
\begin{array}{rcl}
\Psi_{j+1/2} &=& \mathcal{F}(W_{j+1}, W_j) - F(W_j) := F(W^*_{j+1/2}) - F(W_j), \\
\\
\Psi_{j-1/2} &=& F(W_j) - \mathcal{F}(W_j, W_{j-1}) := F(W_j) - F(W^*_{j-1/2}).
\end{array}
\right.
$$

Thanks to the particular structure of Godunov's scheme, we can introduce $\mathcal{J}^*_{j+1/2}$ (resp $\mathcal{J}^*_{j-1/2}$) the Roe average between the states $W^*_{j+1/2}$ and W_j (resp $W^*_{j-1/2}$ and W_j). Calling the averaged entries f of $\mathcal{J}^*_{j+1/2}$ (resp $\mathcal{J}^*_{j-1/2}$) by $\overline{f}^*_{j+1/2}$ and $\underline{f}^*_{j+1/2}$ (resp. $\overline{f}^*_{j-1/2}$ and $\underline{f}^*_{j-1/2}$, and setting $\Delta^*_{j+1/2}(\ .\ ) = (\ .\ )^*_{j+1/2} - (\ .\ )_j$ (resp. $\Delta^*_{j-1/2}(\ .\ ) = (\ .\ )_j - (\ .\ )^*_{j-1/2}$), we can use the formulas (14) with the correct choice of Roe average to define the scheme, namely

$$
\begin{array}{l}
\delta_{j+1/2}\beta = -\nu\overline{u}^*_{j+1/2}\Delta^*_{j+1/2}\beta \\
\\
\delta_{j+1/2}\theta = -\nu\overline{u}^*_{j+1/2}\Delta^*_{j+1/2}\theta \\
\\
\delta_{j-1/2}\beta = -\nu\overline{u}^*_{j-1/2}\Delta^*_{j-1/2}\beta \\
\\
\delta_{j-1/2}\theta = -\nu\overline{u}^*_{j-1/2}\Delta^*_{j-1/2}\theta
\end{array}
\tag{15}
$$

This scheme admits a maximum principle on β and θ under a CFL condition. Mass, momentum and energy are also conserved.

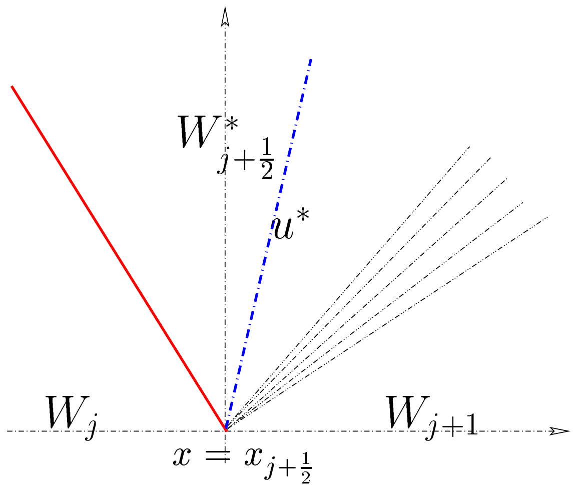

Figure 1. Solution of the Riemann problem between states W_i and $W_{i+1/2}$. $W^*_{j+1/2}$ is the state on the line $x = x_{j+1/2}$.

4. Case of Rusanov scheme

The Rusanov's flux [20] reads

$$F(W_i, W_{j+1}) = \frac{1}{2}\Big(F(W_j) + F(W_{j+1}) - \mu(W_{j+1} - W_j)\Big)$$

so that the residuals can be written as

$$\psi_{j+1/2} = \left(\tfrac{\mathcal{J}_{j+1/2} - \mu_{j+1/2} Id}{2}\right)(W_{j+1} - W_j)$$

$$\psi_{j-1/2} = \left(\tfrac{\mathcal{J}_{j-1/2} + \mu_{j-1/2} Id}{2}\right)(W_j - W_{j-1})$$

so that once more the formula (14) can be used with the functions $\varphi^-(.)$ and $\varphi^+(.)$ redefined by: $\varphi^-(\overline{u}_{j+1/2}) = \frac{\overline{u}_{j+1/2} - \mu_{j+1/2}}{2}$ and $\varphi^+(\overline{u}_{j-1/2}) = \frac{\overline{u}_{j-1/2} + \mu_{j-1/2}}{2}$, namely

$$\begin{aligned}
\delta_{j+1/2}\beta &= -\nu \frac{(\overline{u}_{j+1/2} - \mu_{j+1/2})}{2} \Delta_{j+1/2}\beta \\
\delta_{j+1/2}\theta &= -\nu \frac{(\overline{u}_{j+1/2} - \mu_{j+1/2})}{2} \Delta_{j+1/2}\theta \\
\delta_{j-1/2}\beta &= -\nu \frac{(\overline{u}_{j-1/2} + \mu_{j-1/2})}{2} \Delta_{j-1/2}\beta \\
\delta_{j-1/2}\theta &= -\nu \frac{(\overline{u}_{j-1/2} + \mu_{j-1/2})}{2} \Delta_{j-1/2}\theta
\end{aligned} \tag{16}$$

This scheme admits a maximum principle on β and θ under a CFL condition Mass, momentum and energy are also conserved.

4.1. Time accuracy

We consider a predictor corrector scheme, and assume for simplicity that the predictor and corrector steps are or the form

$$W_j^{n+\alpha} = W_j^n - \alpha\nu \Big(F(W^+_{j+1/2}, W^-_{j+1/2}) - F(W^+_{j-1/2}, W^-_{j-1/2}) \Big) \tag{17}$$

where $\alpha = \frac{1}{2}$ or 1, $W^{\pm}_{j\pm1/2}$ are evaluated via the MUSCL method, but the same type of technique can also be extended to the Harten–Yee's scheme [29]. The trick is to rewrite the scheme in fluctuation form,

$$W_j^{n+\alpha} = W_j^n - \alpha\nu \left(\psi^a_{j+1/2} + \psi^a_{j-1/2} \right)$$

where

$$\psi^a_{j+1/2} = F(W^+_{j+1/2}, W^-_{j+1/2}) - F(W_j) := \psi_{j+1/2} + \psi_{j+1/4}$$

$$\psi^a_{j-1/2} = F(W_j) - F(W^+_{j-1/2}, W^-_{j-1/2}) := \psi_{j-1/2} + \psi_{j-1/4},$$

where $\psi_{j+1/2} = F(W^+_{j+1/2}, W^-_{j+1/2}) - F(W^-_{j+1/2})$, $\psi_{j+1/4} = F(W^-_{j+1/2}) - F(W_j)$, so that we can apply the same machinery as before. If the base scheme is Roe's, Godunov's or Rusanov's, we see that the predictor and corrector are the one given by the formula (14), (15) or (16) evaluated at the corresponding states, and modified by the following corrective term

$$\begin{aligned}
\delta_{j+1/2}\beta &= -\nu \left(\varphi^-(\overline{u}_{j+1/2})\Delta_{j+1/2}\beta + \varphi^-(\overline{u}_{j+1/4})\Delta_{j+1/4}\beta \right) \\
\delta_{j+1/2}\theta &= -\nu \Big(\varphi^-(\overline{u}_{j+1/2})\Delta_{j+1/2}\theta + \varphi^-(\overline{u}_{j+1/4})\Delta_{j+1/4}\theta \Big) \\
\delta_{j-1/2}\beta &= -\nu \left(\varphi^+(\overline{u}_{j-1/2})\Delta_{j-1/2}\beta + \varphi^+(\overline{u}_{j+1/4})\Delta_{j-1/4}\beta \right) \\
\delta_{j-1/2}\theta &= -\nu \Big(\varphi^+(\overline{u}_{j-1/2})\Delta_{j-1/2}\theta + \varphi^+(\overline{u}_{j-1/4})\Delta_{j-1/4}\theta \Big)
\end{aligned} \tag{18}$$

where the functions $\varphi^-(.)$ and $\varphi^+(.)$ depends of the solver used in the predictor (resp corrector) step. We have used the notations:

$$\begin{array}{rcccl}
\Delta_{j+1/2}(.) & = & (.)^+_{j+1/2} & - & (.)^-_{j+1/2}, \\
\Delta_{j-1/2}(.) & = & (.)^+_{j-1/2} & - & (.)^-_{j-1/2}, \\
\Delta_{j+1/4}(.) & = & (.)^-_{j+1/2} & - & (.)_j, \\
\Delta_{j-1/4}(.) & = & (.)_j & - & (.)^+_{j-1/2},
\end{array}$$

$\overline{(.)}_{j\pm1/2}$, $\underline{(.)}_{j\pm1/2}$ the average values between $(.)^+_{j\pm1/2}$ and $(.)^-_{j\pm1/2}$, $\overline{(.)}_{j+1/4}$ and $\underline{(.)}_{j+1/4}$ the average values between $(.)^-_{j+1/2}$ and $(.)_j$, $\overline{(.)}_{j-1/4}$ and $\underline{(.)}_{j-1/4}$ the average values between $(.)_j$ and $(.)^+_{j-1/2}$.

5. Finite volume approximation: General case

In this section, we develop an extension of the previous scheme to multidimensional problems. This introduces additional difficulties that already exist for standard perfect gases slip lines. We first recall the problem, and then we extend our method to 2D problems.

5.1. 2D formulation

Let us recall the partial differential equation (2) defining the behavior of inviscid smooth flow,

$$\left\{\begin{array}{lclclcl} \partial_t\rho & + & \nabla\cdot(\rho\boldsymbol{u}) & & & = & 0\\ \partial_t\boldsymbol{m} & + & \nabla\cdot(\boldsymbol{m}\otimes\boldsymbol{u}) & + & \nabla p & = & 0\\ \partial_t E & + & \nabla\cdot(\rho H\boldsymbol{u}) & & & = & 0\end{array}\right.$$

If $\mathcal{C}$ is any sub-cell of Ω, then for non smooth solutions of the equation (2) becomes:

$$\frac{d}{dt}\int_{\mathcal{C}} W\,dx + \int_{\partial\mathcal{C}} \boldsymbol{F}\,.\,\boldsymbol{n}d\sigma = 0$$

where $\boldsymbol{F}$ is the flux. This formulation suggests the finite volume scheme, where the building block is the solution, exact or approximate, of a Riemann problem,

$$\begin{array}{l}\partial_t W + \partial_n\vec{F} = 0\\ W(\eta=0,\eta^{\perp},t=0) = \left\{\begin{array}{ll} W_L & \text{if } \eta<0\\ W_R & \text{if } \eta>0\end{array}\right.\end{array} \tag{19}$$

where $(\eta,\eta^{\perp})$ are the coordinates in the direct frame $(\boldsymbol{\eta},\boldsymbol{\eta}^{\perp})$ where $||\boldsymbol{\eta}||=1$ and $\boldsymbol{\eta}^{\perp}$ is the unit vector normal to $\boldsymbol{\eta}$ at $M\in\partial\mathcal{C}$. Let us introduce

$$\mathcal{U} = \boldsymbol{u}\cdot\boldsymbol{\eta} \text{ and } \mathcal{V} = \boldsymbol{u}\cdot\boldsymbol{\eta}^{\perp}.$$

This system reads

$$\begin{array}{l}\partial_t\rho + \partial_\eta(\rho\mathcal{U}) = 0\\ \partial_t\rho u + \partial_\eta(\rho u\mathcal{U}) + \eta_x\partial_\eta p = 0\\ \partial_t\rho v + \partial_\eta(\rho v\mathcal{U}) + \eta_y\partial_\eta p = 0\\ \partial_t E + \partial_\eta(\rho\mathcal{U}H) = 0\end{array} \tag{20}$$

and by simple manipulations, we get

$$\begin{array}{l}\partial_t\rho + \partial_\eta\rho\mathcal{U} = 0\\ \partial_t\rho\mathcal{U} + \partial_\eta(\rho\mathcal{U}^2) + \partial_\eta p = 0\\ \partial_t\rho\mathcal{V} + \partial_\eta(\rho\mathcal{U}\mathcal{V}) = 0\\ \partial_t E + \partial_\eta(\rho\mathcal{U}H) = 0.\end{array} \tag{21}$$

The numerical fluxes are constructed from (20). However, this has some drawbacks. As pointed out in [27], the computations of slip lines can be inaccurate. If one consider for example a slip line initially aligned with the mesh, like on Figure 2, where the normal velocity is non zero, then even for a perfect gas, it is easy to see that for any upwind solver, the pressure will not remain uniform. This phenomena is quite similar to what happens for mixture of perfect gases and is due to the non correct computation of the tangential velocity. This pollutes the evaluation of the kinetic energy, and then that of the pressure. In the case of mixture of gases or the stiffened equation of state, this phenomena may lead to the blow up of the calculation, for example when $v_L - v_R$ is large, see [23] for example. The scheme proposed in [23] used a cartesian mesh and the multidimensional scheme uses a splitting technique.

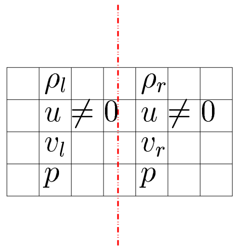

Figure 2. Slip line configuration.

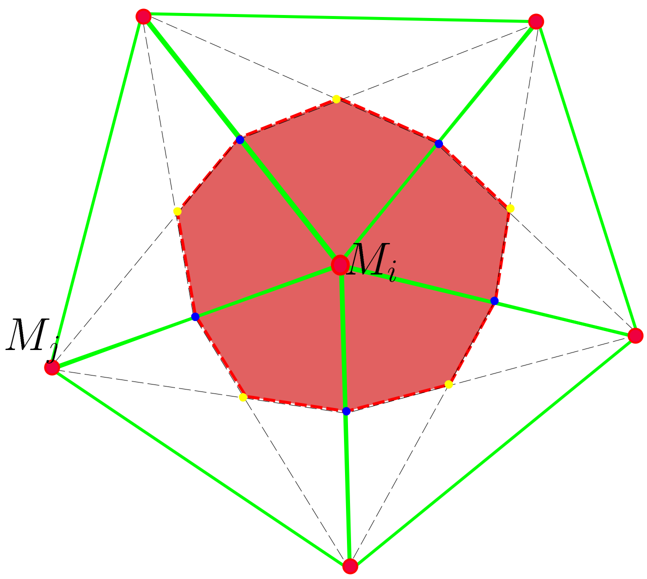

Figure 3. Dual cell C_i associated with triangulation vertex M_i in 2-D space

5.2. Numerical method

The strategy we develop relies on a conservative numerical flux that discretise the 2D version of (2). The scheme, for the conserved variables $W = (\rho, \boldsymbol{m}, E)^T$ is

$$W_i^{n+1} = W_i^n - \frac{\delta t}{a_i} \sum_{j \in \vartheta(i)} \phi_{ij} \tag{22}$$

where δt is the time step, a_i the area of the cell (see figure 3), $\vartheta(i)$ the set of the neighboring cells of the cell i and ϕ_{ij} the fluctuation associated to the cell interface (ij). This fluctuation is computed from the solution of a Riemann problem at the cell interface.

We introduce the additional notations:

$$\mathcal{Q} = \tfrac{\boldsymbol{u}\cdot\boldsymbol{u}}{2}, \quad \mathcal{Q}^\perp = \tfrac{\mathcal{V}^2}{2}$$

$$\mathcal{W} = (\rho,\ \rho\mathcal{U},\ E)^{\mathrm{T}}, \quad \mathcal{F} = (\rho\mathcal{U},\ \rho\mathcal{U}^2 + p,\ \rho H\mathcal{U})^{\mathrm{T}}, \quad \mathcal{Z} = (\mathcal{W},\ \rho\mathcal{V})^{\mathrm{T}}$$

The system (4), in the local coordinates is given by:

$$\begin{cases} \partial_t \mathcal{W} + \partial_\eta \mathcal{F} = 0, \\ \partial_t(\rho\mathcal{V}) + \partial_\eta(\rho\mathcal{U}\mathcal{V}) = 0, \\ \partial_t(\rho\mathcal{Q}^\perp) + \partial_\eta(\rho\mathcal{U}\mathcal{Q}^\perp) = 0, \\ \beta p + \theta = E - \dfrac{\rho\mathcal{U}^2}{2} - \rho\mathcal{Q}^\perp \end{cases} \tag{23}$$

This system has more equations than it is need. Indeed, the equation on the tangential momentum $(\rho\mathcal{V})$ or the equation on the tangential kinetic energy $(\rho\mathcal{Q}^\perp)$ can be obtained by a combination of the other equations:

$$\partial_t(\rho\mathcal{Q}^\perp) = \mathcal{V}\partial_t(\rho\mathcal{V}) - \frac{\mathcal{V}^2}{2}\partial_t\rho \tag{24}$$

The equation satisfied by the tangential kinetic energy is redundant in the continuous formulation, *but in general it is not numerically satisfied.* This is the cause of pressure oscillations in multidimensional flow problems [27,23]. The idea is to discretize the tangential kinetic equation, and to use this discretisation in order to compute correctly the pressure. Hence, we will locally use this equation to achieve a consistent approximation of the pressure near contact discontinuities with non constant tangential velocity.

We now illustrate the numerical approach in the case of a Roe type scheme characterized by an upwind function φ. In the sequel we use the notations of Annex B. As pointed out in section 3, the method can easily be extended to Godunov and Rusanov' schemes, following the same ideas as in §3. The construction of Roe scheme in 2D is sketched in Annex B. The numerical dissipation of Roe scheme is

$$\begin{aligned} \varphi(\tilde{\mathcal{J}})\Delta Z = \ & \varphi(\overline{\mathcal{U}})\left(\Delta(\rho) - \xi\right)\boldsymbol{r}_1 \\ & + \varphi(\overline{\mathcal{U}} - \tilde{c})\left(\tfrac{\xi - \Theta}{2}\right)\boldsymbol{r}_2 + \varphi(\overline{\mathcal{U}} + \tilde{c})\left(\tfrac{\xi + \Theta}{2}\right)\boldsymbol{r}_3 \\ & + \varphi(\overline{\mathcal{U}})\left(\underline{\rho}\Delta(\mathcal{V})\right)\boldsymbol{r}_4 + \varphi(\overline{\mathcal{U}})\tfrac{\underline{\rho}\Delta\beta}{\overline{\beta}}\boldsymbol{r}_5 + \varphi(\overline{\mathcal{U}})\tfrac{\overline{\beta}\Delta\theta - \overline{\theta}\Delta\beta}{\underline{\rho}\overline{\beta}}\boldsymbol{r}_6 \end{aligned} \tag{25}$$

Then, according to the consistency with the integral form, the fluctuation $\mathbf{\Psi}_{ij}$ at the cell interface is given by:

$$\mathbf{\Psi}_{ij} = \frac{1}{2}\left\{\Delta\mathcal{G} - \varphi(\tilde{\mathcal{J}})\Delta Z\right\} = \varphi^{-}(\tilde{\mathcal{J}})\Delta Z = \begin{pmatrix} \mathbf{\Psi}_{ij}^{\mathcal{Z}} \\ \mathbf{\Psi}_{ij}^{\rho\beta} \\ \mathbf{\Psi}_{ij}^{\rho\theta} \end{pmatrix} = -\mathcal{G}_i + \mathbf{\Phi}_{ij} \tag{26}$$

Therefore, the update of the conservatives variables W on the internal cells, is:

$$W_i^{n+1} = W_i^n - \frac{\delta t}{a_i}\sum_{j\in\vartheta(i)} \mathcal{M}_{ij}^{-1}\mathbf{\Psi}_{ij}^{\mathcal{Z}} = \sum_{j\in\vartheta(i)} \frac{a_{ij}}{a_i}\mathcal{M}_{ij}^{-1}\mathcal{Z}_{ij}^{n+1}$$

where $\mathcal{Z}_{ij}^{n+1} = \mathcal{Z}_{ij}^{n} - \frac{\delta t}{a_{ij}}\mathbf{\Psi}_{ij}^{\mathcal{Z}}$, δt is the time step, a_i the area of the cell, a_{ij} the component of the cell area associated to the interface and $\vartheta(i)$ the set of the neighboring cells of the cell i, see Figure 4. We denote by Ψ_{ij} the first three components of $\mathbf{\Psi}_{ij}^{\mathcal{Z}}$ and obtain:

$$\mathcal{W}_{ij}^{n+1} = \mathcal{W}_{ij}^{n} - \frac{\delta t}{a_{ij}}\Psi_{ij} \tag{27}$$

This relation will gives the updated variables associated to the sub-cell a_{ij} of the cell a_i. Therefore, the projection on the cell a_i of the variables is obtained by averaging the sub-cells variables weighted by the ratio $\frac{a_{ij}}{a_i}$. This is one of the keys of the approach proposed in this paper. Indeed, with this decomposition, we can focus the study on the sub-cells a_{ij} : The situation is now very similar to the 1-D case.

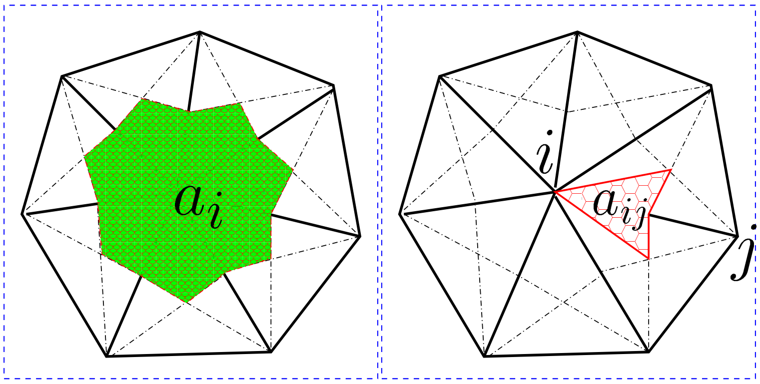

Figure 4. Area (a_i) of the cell and partial area (a_{ij}) associated to a given segment (i, j).

Let us denote $\delta X_{ij} = X_{ij}^{n+1} - X_{ij}^{n}$ and

$$K = \rho\mathcal{Q} = \frac{1}{2}\rho\mathcal{U}^2 + \frac{1}{2}\rho\mathcal{V}^2 = \mathcal{K} + K^{\perp}.$$

Here, the local frame is defined by the normal to a_{ij} at the interface between the cells a_i and a_j, and the orthogonal vector, such that the frame is direct. We have

$$\delta E_{ij} = \delta(\rho\epsilon)_{ij} + \delta K_{ij}^{\perp} + \delta\mathcal{K}_{ij}, \quad \delta\mathcal{K}_{ij} = \frac{1}{2}\left(\rho_{ij}^{n+1}\mathcal{U}_{ij}^{n+1}\delta\mathcal{U}_{ij} + \mathcal{U}_{ij}^{n}\delta(\rho\mathcal{U})_{ij}\right)$$

and $\delta(\rho\mathcal{U})_{ij} = \rho_{ij}^{n+1}\delta\mathcal{U}_{ij} + \mathcal{U}_{ij}^{n}\delta\rho_{ij}$. For simplicity, we denote:

$$\mathcal{Q}_{ij}^{*\|} = \frac{\mathcal{U}_i^n\mathcal{U}_{ij}^{n+1}}{2}, \quad \mathcal{U}_{ij}^{*} = \frac{\mathcal{U}_{ij}^{n+1} + \mathcal{U}_i^n}{2} \text{ and } \boldsymbol{\ell}_{ij} = (\mathcal{Q}_{ij}^{*\|},\ -\mathcal{U}_{ij}^{*},\ 1)^{\mathrm{T}}.$$

Therefore, $\delta(\rho\epsilon)_{ij} + \delta K_{ij}^{\perp} = \mathcal{Q}_{ij}^{*\|}\delta\rho_{ij} - \mathcal{U}_{ij}^{*}\cdot\delta(\rho\mathcal{U})_{ij} + \delta E_{ij}$ so that denoting $\sigma_{ij} = \delta t/a_{ij}$

$$\beta_{ij}^{n+1}\delta p_{ij} + p_i^n\delta\beta_{ij} + \delta\theta_{ij} + \delta K_{ij}^{\perp} = -\sigma_{ij}\boldsymbol{\ell}_{ij}\cdot\Psi_{ij} \tag{28}$$

Setting $\varphi^{\pm}(X) = \frac{X\pm\varphi(X)}{2}$, the components of the numerical fluctuation are given by:

$$\begin{aligned}
\Psi_{ij}^{\rho} &= \varphi^{-}(\overline{\mathcal{U}})\left(\Delta\rho - \xi\right) + \tilde{c}\left(\alpha_1^{-}\xi + \alpha_2^{-}\Theta\right)\\
\Psi_{ij}^{\rho\mathcal{U}} &= \overline{\mathcal{U}}\Psi_{ij}^{\rho} \quad + \quad \Psi_{ij}^{p}\\
\Psi_{ij}^{E} &= \overline{H}\Psi_{ij}^{\rho} \quad + \quad \delta
\end{aligned}$$

where $\Psi_{ij}^{p} = \tilde{c}^2\left(\alpha_2^{-}\xi + \alpha_1^{-}\Theta\right)$,

$$\delta = \overline{\mathcal{U}}\Psi_{ij}^{p} + \varphi^{-}(\overline{\mathcal{U}})\Big(-\overline{\beta}\tilde{c}^2\left(\Delta\rho - \xi\right) + \underline{\rho}\overline{\mathcal{V}}\Delta\mathcal{V} + \underline{p}\Delta\beta + \Delta\theta\Big),$$

$$\alpha_1^{-} = \frac{\varphi^{-}(\overline{\mathcal{U}}+\tilde{c}) + \varphi^{-}(\overline{\mathcal{U}}-\tilde{c})}{2\tilde{c}}, \quad \alpha_2^{-} = \frac{\varphi^{-}(\overline{\mathcal{U}}+\tilde{c}) - \varphi^{-}(\overline{\mathcal{U}}-\tilde{c})}{2\tilde{c}}$$

Using these expressions of the fluctuations associated to the edge (i,j), we compute:

$$\begin{aligned}
\boldsymbol{\ell}_{ij}\cdot\Psi_{ij} \;=\;& \mathcal{S}_{ij} + \overline{\beta}\left(\tilde{c}\alpha_1^{-}\Delta p + \alpha_2^{-}\underline{\rho}\tilde{c}^2\Delta\mathcal{U}\right) + \varphi^{-}(\overline{\mathcal{U}})\left(p_i\Delta\beta + \Delta\theta\right)\\
&+\tilde{\mathcal{Q}}^{\perp}\Psi_{ij}^{\rho} + \varphi^{-}(\overline{\mathcal{U}})\underline{\rho}\overline{\mathcal{V}}\Delta\mathcal{V}
\end{aligned} \tag{29}$$

where

$$\mathcal{S}_{ij} = \left(\mathcal{Q}_{ij}^{*\|} - \mathcal{U}_{ij}^{*}\overline{\mathcal{U}} + \tilde{\mathcal{Q}}^{\|}\right)\Psi_{ij}^{\rho} + \Psi_{ij}^{p}\left(\overline{\mathcal{U}} - \mathcal{U}_{ij}^{*}\right) + \varphi^{-}(\overline{\mathcal{U}})\left(\underline{p} - p_i\right).$$

In general, $\mathcal{S}_{ij}$ is consistent with zero and equal to zero if the velocity and the pressure field is a space-time constant. $\sigma_{ij}\tilde{\beta}\tilde{c}\alpha_1^{-}\Delta p$ is consistent with $\beta\mathcal{U}\partial_\eta p$ and $\sigma_{ij}\tilde{\beta}\alpha_2^{-}\underline{\rho}\tilde{c}^2\Delta\mathcal{U}$ is consistent with $\beta\rho c^2\partial_\eta\mathcal{U}$. Therefore a natural discretisation of the EOS parameters is obtained by a combination of equations (28)-(29) and an identification of the different terms with respect to the non conservative formulation in the direction $\boldsymbol{\eta}_{ij}$:

$$\delta\beta_{ij} = -\sigma_{ij}\varphi^{-}(\overline{\mathcal{U}})\Delta_{ij}\beta \quad \text{and} \quad \delta\theta_{ij} = -\sigma_{ij}\varphi^{-}(\overline{\mathcal{U}})\Delta_{ij}\theta \tag{30}$$

If we denote $\delta\beta_{ji}$ and $\delta\theta_{ji}$ the variations on the cell j associated to the interface, it is easy to see that: $\delta\beta_{ji} = -\sigma_{ji}\varphi^{+}(\overline{\mathcal{U}})\Delta_{ij}\beta$ and $\delta\theta_{ij} = -\sigma_{ji}\varphi^{+}(\overline{\mathcal{U}})\Delta_{ij}\theta$ where $\sigma_{ji} = \delta t/a_{ji}$.

These relations are obtained under the assumption that the update of the tangential kinetic energy is consistent in the following way:$\delta K_{ij}^{\perp} \simeq -\sigma_{ij}\left(\tilde{\mathcal{Q}}^{\perp}\Psi_{ij}^{\rho} + \varphi^{-}(\overline{\mathcal{U}})\underline{\rho}\overline{\mathcal{V}}\Delta\mathcal{V}\right)$. We set

$$\Psi_{ij}^{K^{\perp}} = \tilde{\mathcal{Q}}^{\perp}\Psi_{ij}^{\rho} + \varphi^{-}(\overline{\mathcal{U}})\underline{\rho}\overline{\mathcal{V}}\Delta\mathcal{V} \tag{31}$$

eventhough we have noticed that the really important thing is to have a consistent discretisation of the tangential kinetic equation to define $\Psi^{\perp}_{ij}$. Because the stability of the contact discontinuity is marginal in 2D and 3D [25], this consistency is generally violated when the tangential velocity is not continuous, even for perfect gaz EOS. Let us consider the following consistent discretisation of the tangential kinetic energy: $(K^{\perp}_{ij})^{n+1} = (K^{\perp}_{ij})^n - \sigma_{ij}\Psi^{K^{\perp}}_{ij}$. In order to take into account this consistency in the numerical approach, we define a local update of the internal energy $\rho\epsilon$ by:

$$(\rho\epsilon)^{n+1}_{ij} = E^{n+1}_{ij} - \frac{(\rho^{n+1}_{ij}\mathcal{U}^{n+1}_{ij})^2}{2\rho^{n+1}_{ij}} - (K^{\perp}_{ij})^{n+1} \simeq E^n_i - K^n_i - \sigma_{ij}\Psi^E_{ij} + \sigma_{ij}\Psi^K_{ij}$$

where

$$\Psi^K_{ij} = \Psi^{K^{\perp}}_{ij} + \mathcal{U}^n_i\Psi^{\rho\mathcal{U}}_{ij} + \frac{(\mathcal{U}^n_i)^2}{2}\Psi^{\rho}_{ij} - \frac{\sigma_{ij}\Psi^{\rho\mathcal{U}}_{ij}}{2\rho^n_i}\left(\Psi^{\rho\mathcal{U}}_{ij} + 2\mathcal{U}^n_i\Psi^{\rho}_{ij}\right)$$

From this discretization, we can construct an average internal energy on the cell with is locally consistent. But, this energy is different to the one that can be computed from the conservative variables on the cell at the time t^{n+1}. Therefore we propose to update the total energy by the value $\hat{E}^{n+1}_i$ satisfying the relation:

$$\sum_{j\in\vartheta(i)} \frac{a_{ij}}{a_i}(\rho\epsilon)^{n+1}_{ij} = \hat{E}^{n+1}_i - \frac{\boldsymbol{m}^{n+1}_i\cdot\boldsymbol{m}^{n+1}_i}{2\rho^{n+1}_i}$$

This means that the modified value of the energy at the time t^{n+1} is given by a non conservative formulation :

$$\hat{E}^{n+1}_i = E^n_i - \frac{\delta t}{a_i}\sum_{j\in\vartheta(i)}\left(\Psi^E_{ij} - \Psi^K_{ij}\right) + \frac{\boldsymbol{m}^{n+1}_i\cdot\boldsymbol{m}^{n+1}_i}{2\rho^{n+1}_i} - \frac{\boldsymbol{m}^n_i\cdot\boldsymbol{m}^n_i}{2\rho^n_i}$$

The update of the material parameters in the cell is defined as follows :

$$\beta^{n+1}_i = \beta^n_i - \frac{\delta t}{a_i}\sum_{j\in\vartheta(i)}\varphi^-(\overline{\mathcal{U}})\Delta_{ij}\beta, \quad \text{and} \quad \theta^{n+1}_i = \theta^n_i - \frac{\delta t}{a_i}\sum_{j\in\vartheta(i)}\varphi^-(\overline{\mathcal{U}})\Delta_{ij}\theta \qquad (32)$$

The numerical scheme is then defined by the classical conservative formulation for the mass and momentum. The total energy update is obtained by a non conservative formulation. The material parameters and the mean pressure are given by (32). The resulting non conservative scheme is a more general formulation of the idea developed in [24] with a splitting approach. Similar procedure is used in [3] : the important variables are the primitive variables and not the conservative ones. To illustrate this point, we present a quasi-1D test case where this default affects considerably the solution of the Euler equation in 2D, see Figure 9.

6. The reactive model

We now detail the extension of this method for materials that the physical state changes during chemical reaction: solid energetic materials. This can easily be done because the formulation is the *same* everywhere.

Solid explosives start from the solid state before reaction, then become a solid-gas mixture during reaction and a pure gas mixture at the end of the reaction. We first give some basis regarding the thermodynamics of such materials. We then give the some elements regarding their chemistry. We finally detail the way to account of the equation of state changes during the decomposition process and the way to couple it with the numerical treatment of the interfaces. This is important for all applications involving interactions of detonations with neighboring materials.

6.1. Flow model

When dealing with detonation waves in condensed explosives the pressure and velocity conditions are so high that liquids and solids become compressible and governed by the gas dynamics equations. Thus, system (2) becomes valid even for solids. The closure of such system is achieved by equation (1) that needs some modifications to account for changes in chemical composition of the mixture. This will be detailed in the next subsection. However, let us mention that the system (2) is not sufficient when solving detonation waves with an Eulerian method as detailed previously. It must be complemented by an equation allowing the determination of the phases concentration, varying inside the reaction zone of the detonation wave. We define the gas volume fraction λ, whose initial value is zero in the solid explosive and that tends to the unity at the end of the reaction. The explosive being moving, the volume fraction equation reads:

$$\partial_t \rho\lambda + \nabla.(\rho u \lambda) = \rho\dot{\lambda} f \tag{33}$$

where $\dot{\lambda}$ represents the rate of creation of the gas phase. Assuming that the rate of decomposition obeys a simple pressure kinetics (Vieille law), we get:

$$\dot{\lambda} = (1-\lambda) a p^n \tag{34}$$

where a and n are the kinetics parameters of the explosive. The function f is an indicator that allows the determination of the explosive concentration in the mesh. Indeed, the decomposition law must be applied only at points where the explosive is present and not in inert materials. Spatial localization of the explosive is realized by the introduction of function f that equals zero initially everywhere, except in the explosive where it equals 1. Its evolution is given by:

$$\partial_t \rho f + \nabla.(\rho u f) = 0 \tag{35}$$

6.2. Mixture equation of state

During the reaction process the explosive passes from solid state to gaseous products. The equation of state (1) must be reformulated to deal with this transformation. During the detonation propagation, there are three states in the flow: state 1 where the solid explosive is intact, state 2 where the explosive is completely reacted and composed exclusively of gases and an intermediate state composed of a mixture of solid and gases inside the reaction zone. To deal with this various states we propose a mixture equation of state able to reproduce all of them in a unique formulation. Each pure fluid is assumed to obey the stiffened gas EOS. Thus the internal energy of the solid reads

$$\epsilon_s = \frac{\beta_s + \theta_s}{\rho_s} + c_s \ \text{ with } \ c_s = \epsilon_{s0} - \frac{\theta_s}{\rho_{s0}},$$

where ϵ_{s0}, c_s and ρ_{s0} are respectively the formation energy of the solid, the internal energy and density under standard conditions. For the gas phase, we assume the same formulation but instead of choosing standard conditions as reference, we retain the Chapman-Jouguet (CJ) point. Thus the internal energy reads

$$\epsilon_g = \frac{\beta_g + \theta_g}{\rho_g} + c_g \ \text{ with } \ c_g = \epsilon_{cj} - \frac{\theta_{cj}}{\rho_{cj}},$$

where $\theta_{cj} = \frac{p_{cj}+\gamma_g p_{\infty,g}}{\gamma_g - 1}$ and the characteristics states ρ_{cj}, ϵ_{cj} a nd p_{cj} can be obtained from a thermochemical code like CHEETAH [7].

With the internal energies definition, the mixture equation of state is readily obtained under the assumption of pressure equilibrium between phases. This assumption is justified because of the small size of the solid particles into the mixture and of the high speed of sound of both two phases. Indeed, the pressure relaxation time is closed to the time required for an acoustic wave to cross a solid grain diameter. The mixture internal energy reads:

$$\rho\epsilon = \lambda\rho_g\epsilon_g + (1-\lambda)\rho_s\epsilon_s \tag{36}$$

and now ϵ is a function of ρ, p and λ. According to the previous definitions for the internal energies (ϵ_s and ϵ_g) and assuming that gas and solid are at the same pressure $p = p_g = p_s$, we recover an EOS of the same type as the pure phases. It reads

$$\epsilon = \frac{\beta+\theta}{\rho} + c \quad \text{with} \quad \left\{ \begin{array}{rl} c(\lambda) = & \lambda c_g + (1-\lambda)c_s, \\ \beta(\lambda) = & \lambda\beta_g + (1-\lambda)\beta_s, \\ \theta(\lambda) = & \lambda\theta_g + (1-\lambda)\theta_s. \end{array} \right. \tag{37}$$

It is now necessary to determine the decomposition parameters of the kinetics law of the explosive (parameters of the Vieille law).

6.3. Chemical kinetics

The parameters of the Vieille's law are not the standard ones as determined in stand burner or closed bomb. Indeed, the parameters determined by such a way are those of the deflagration regime of the explosive. At the pressure levels we are interested in, these parameters cannot be determined by direct measurement. Also, the kinetic parameters we are looking for are not related to the ignition and transition regime of the explosive. Such mechanisms cannot be summarized in a simple Vieille law [17]. The kinetics parameters needed here are related only to the self detonation propagation regime of the explosive.

To determine these parameters we use an experimental observation based on the front curvature of the detonation wave. The energy responsible for the front propagation is liberated between the shock front and the sonic plane (in the frame of reference related

to the shock front). The distance between these two planes being finite, multidimensional rarefaction waves coming from the boundaries of the explosive product are able to propagate inside the reaction zone of the explosive. These effects result in a curvature of the shock front. Thus, it is clear that the shock curvature is a result of the coupling effects between the chemical kinetics of the explosive and the various hydrodynamics effects, especially the rarefaction waves.
Considering a cylindrical charge of given diameter, the corresponding detonation wave propagates at a given velocity with a given curvature. By measuring these variables for various charge diameters we obtain a relation between the front curvature and its velocity. This relation is intrinsic to the explosive. It is a result of its chemical kinetics and rarefaction waves. This relation will enable us to determine the kinetics parameters in a wide range of pressures. Indeed, when the diameter varies, the detonation velocity and the pressure inside the reaction zone vary strongly.
By using the equation of state for the mixture, combined with system (2) and equation (33) in the context of a steady two-dimensional axi-symmetric flow in the frame of the shock and specialized onto the symmetry axis, we get an ODE system easy to solve. It corresponds to the Wood and Kirkwood model [5]. Giving an arbitrary guess for the chemical kinetics parameter of the Vieille's law and the front curvature for a given charge diameter this model furnishes the corresponding stable detonation velocity. This detonation velocity accounts for the coupling between the hydrodynamics and the chemical kinetics. The kinetics parameter may be varied in order to reach the experimental detonation velocity. This type of process may be done for all front curvatures, that is for all charge diameters. When the computed detonation velocities and the experimental ones are in good agreement for any front curvature, the kinetics parameters are determined. This type of inverse procedure is detailed in [18] and [21].

6.4. Numerical approach for the reactive model

In the reactive case, the equation of state (37) is now a function of three variables. The mixture internal energy can be written as: $\epsilon = e + c$. Thus the total energy equation $\partial_t E + \nabla.(\rho H \boldsymbol{u}) = 0$ can be put under the form

$$\partial_t E^* + \nabla.(\rho H^* u) = -\rho\dot{\lambda}c'$$

with $E^* = \rho e + \rho\frac{\boldsymbol{u}\cdot\boldsymbol{u}}{2}$ and for any variable $(\cdot)' = \frac{d(\cdot)}{d\lambda}$. The contribution $-\rho\dot{\lambda}c'$ is related to the combustion energy release. The equations governing the material interfaces motion must also be modified. Indeed, in the reactive case, the material parameters β and θ of equation (37) now depend on the volume fraction λ. Therefore, the materials parameters are governed by the equations:

$$\partial_t\beta + \boldsymbol{u}\cdot\nabla\beta = f\dot{\lambda}\beta' \quad \text{and} \quad \partial_t\theta + \boldsymbol{u}\cdot\nabla\theta = f\dot{\lambda}\theta' \tag{38}$$

To summarize, in the reactive case, the overall system to solve reads:

$$\left\{\begin{array}{l}\partial_t\rho+\nabla(\rho\boldsymbol{u})=0\\ \partial_t\rho\boldsymbol{u}+\nabla(\rho\boldsymbol{u}\otimes\boldsymbol{u})+\nabla p=0\\ \partial_t E^*+\nabla(\rho H^*\boldsymbol{u})=-\rho\dot{\lambda}c'\\ \partial_t\rho f+\nabla(\rho f\boldsymbol{u})=0\\ \partial_t\rho\lambda+\nabla(\rho\lambda\boldsymbol{u})=\rho\dot{\lambda}f\\ \partial_t\rho\beta+\nabla(\rho\beta\boldsymbol{u})=\rho f\dot{\lambda}\beta'\\ \partial_t\rho\theta+\nabla(\rho\theta\boldsymbol{u})=\rho f\dot{\lambda}\theta'\end{array}\right. \tag{39}$$

The overall system is split into a convective one and an ODE system. The convective part of this system is solved by the hyperbolic solver detailed in the preceding sections. The source terms are then accounted for by an appropriate ODE solver.

7. Numerical experiments

The technique developed in this paper is now applied to three tests cases : a water-air shock tube, an interaction of a shock with an air bubble in water and a detonation wave. The computations are performed with two dimensional unstructured meshes for the two first cases and with structured meshes for the last one. In any cases, the methodology developped in the framework of unstructured grids is applied and a second order accurate MUSCL explicit scheme is used.

7.1. Water-Air shock Tube

We consider a square domain of $1m \times 1m$ length. Initially there is a material interface, located at $x = 0.7m$, separating two fluids: water at the left and air at the right. The two fluids are initially at rest and there is a jump on the density, the pressure and the material parameters (β and θ). The solution of this Riemann problem is composed by a shock wave traveling in the air, a rarefaction traveling in the water and the material interface (contact discontinuity) [9]. The explicit second order accurate scheme used here is based on the classical Roe's solver with CFL=0.75. Computations of the first test case (Fig 5) are performed on an unstructured mesh of 4506 vertices with about 750 vertices in the wave propagating direction. The numerical results have a good agreement with the analytical solution. For the sake of clarity, only the numerical solutions, at the final time $T = 230\mu s$, are plotted (Fig: 7,6). The one-dimensional structure of the one dimensional analytical solution is preserved (Fig: 7) by this modified conservative approximation. Moreover, there are no oscillations at the material interface (Fig: 7,6).

The solution with the coarse mesh (1782 vertices) is less accurate but the global profile of the waves are captured (Fig: 8). The solution of the second test case (Fig 9) is, analytically, composed by the solution of the test case one and a strong contact discontinuity on the v component of the velocity. When a conservative scheme is used (Roe, Rusanov or HLL solvers), numerical result produce a shock wave traveling faster than the exact one. This is a consequence of the lack of accuracy, on the tangential velocity (v), produced by the conservative schemes. Indeed, the pressure and the sound speed, used to numerically compute the waves speed, are directly related to the modulus of the velocity. Computations performed on structured or unstructured meshes with first or second order accurate conservative schemes give rise to the same problem (Fig 10). We have also computed some numerical solutions with the partially non conservative scheme. Therefore, the numerical results, computed with this non conservative scheme (Fig 10), are very close to the analytical one.

7.2. Shock-bubble interaction.

In this section we investigate the dynamics of a shock-bubble interaction. The size of the computational domain is 20×10 centimeter, with absorption boundary conditions on the right and piston conditions on the left. The initial flow is water at rest with an cylindrical air bubble, of $4cm$ radius, centered at the point (5, 5)cm. The system is at the equilibrium with uniform pressure and velocity then a shock wave is produced at the left of the domain by the piston motion (Figure 11). In this test case, an unstructured mesh of 98489 nodes and 195776 triangles is used. Numerical results are computed with an explicit second order accurate scheme based on the Roe solver and the CFL=0.5. In this computation, the material interface is not explicitly defined.

The speed of sound inside the air bubble is smaller than that of the surrounding water. After the first interaction with the bubble, the incident shock wave is diffracted into two waves (Figure 12): a reflected rarefraction wave moving from right to left in the water and a transmitted shock wave in the bubble. Later, when the incident wave have passed the bubble, we can observe the multiple scattering phenomena that is developped (Figures 13 and 14). Due to the fact that air compressibility is larger than the water one, the downstream bubble interface is almost motionless during the compression (Figure 17). Let us denote that the numerical scheme preserves this material interface and no spurious oscillations or non physical states are produced during the computation.

Then, the transmitted shock emerges in the water (Figure 15 for $t \simeq 18.5ms$) and deforms the downstream material front. Two pairs of vortices (Figures 16 and 17) are produced arround the compressed air bubble. The upstream interface is folded and progressivelly a re-rentrant jet is formed. This jet breaks the bubble in two parts and drives them downstream (Figure 18). Even if the context is not the same, the behavior of the shock-bubble obtained in this investigation is similar to the experiments realized in [13].

7.3. Detonation wave

We consider a cylindrical Plexiglas tube filled with a solid explosive. The tube is surrounded by air. The explosive is a mixture of ammonium nitrate, fuel, water and other minor compounds. It is a non ideal explosive: its chemical decomposition rate is very slow compared to standard solid high explosives. Consequently the consideration of the chemical kinetics effects are very important for the detonation propagation and its effects over structures. The configuration studied consists in several Plexiglas tubes of different diameter. The tube thickness is 3mm. The initial density of Plexiglas is $1186kg/m^3$ and the parameters of the equation of state are $\gamma = 3.8$ and $p_\infty = 2 \times 10^9 Pa$. The EOS parameters for the solid state of the explosive are: $\epsilon_{s0} = 0$, $\gamma_s = 2.9$, $p_{\infty_s} = 4.5 \times 10^8 Pa$ and the initial density is $\rho_0 = 1000kg/m^3$. The EOS parameters of the detonation products are: $\gamma_g = 2.37$, $p_{\infty_g} = 0$, $p_{CJ} = 11 \times 10^9 Pa$, $D_{CJ} = 5875m/s$ and $\rho_{CJ} = 1477kg/m^3$. The Chapmann Jouguet (CJ) state is obtained by a thermochemical equilibrium computation using CHEETAH [7]. Finally the kinetics parameter of equation (34) are $a = 3.34 \times 10^{-3} Pa^{-n}$ and $n = 0.8$ when $p > p_0$ and $a = 0$ otherwise. The threshold pressure p_0 is take equal to $1GPa$. The following computation is performed with a mesh of 300×75 cells and we first consider a cylindrical charge of 84mm diameter. The computational domain is 30 cm long and 6 cm high. The results are shown when the stable detonation state is obtained (19). The detonation front is clearly visible as well as the expansion of the Plexiglas cylinder. These results are to compare with X rays measurements as shown on Figure 20. The qualitative agreement between the computations and experiment can be noticed. The quantitative comparison will be given after examining the effects of the charge size. We now consider another charge of 174mm internal diameter. The mesh involves now 400×150 cells. The computed density contours are shown on Figure 21. Again, the shock front and tube expansion are clearly visible. The numerical data are now compared with the experimental ones on the Table 8. From these results an excellent agreement can be noticed. It is important to note the wide range of variation of the detonation velocity compared to the ideal one ($5875m/s$). This is a result of the coupling effects between the low rate of the chemical kinetics of this explosive, and the rarefaction waves traveling inside the reaction zone.

8. Conclusion

In the case of the stiffened gas EOS, we have pointed out the different problems arising in the computation of the multidimensional mutimaterial flows: The pressure can become oscillatory across slip lines, and consequently the velocity and the other variables too. For very different EOS, and/or extreme flow configurations this leads to the breakdown of the code. The situation is even worse in several space dimensions because the kinetic velocity is not accurately computed around slip lines.

We have discussed these different problems and propose solutions. They amount to a slight modification of existing schemes ; they are easily incorporated into existing codes. These modifications are of two types : first the identification of the numericaly pertinent thermo-dynamical parameters that have to be updated, second more consistent calculation of the kinetic energy. We note that the second ingredient of the method arises because of the multidimensional nature of the problems and the class of conservative schemes (directional splitting or finite volume approach) we consider here. The drawback of our method is that the scheme is not any longer strictly conservative on the total energy. We note however that the loss of conservation occur only around slip lines and does not seem to pollute the solutions. The method is flexible, it is applicable on any type of mesh : Cartesian, unstructured, hybrid, because of a local formulation.

Several numerical examples, with and without the corrections, are presented. They demonstrate the efficiency of our method on triangular unstructured meshes.

Acknowledgments
This paper has been completed during the CEMRACS 2000 summer school, held at CIRM (Marseilles) during the summer 2000. The third author has also been partially supported by NITROCHIMIE. He addresses special thanks to S. Mencacci and T. Rousse. The experiments shown for the detonation problem have been done at CEA/DAM Moronvilliers and we particularly thank G. Rodriguez.

REFERENCES

1. R. Abgrall. Generalisation of the Roe scheme for the computation of a mixture of perfect gases. *La Recherche Aérospatiale*, **6**, Dec 1988.
2. R. Abgrall. How to prevent pressure oscillations in multicomponent flows : a quasi conservative approach. *J. Comp. Phys.*, **125**, pp. 150–160, Sept. 1996.
3. R. Abgrall and S. Karni. Compressible multifluids. *J. Comput. Phys.*, **169**, no 2, pp. 594-623, May, 2001.
4. D. Chargy, R. Abgrall, L. Fezoui, and B. Larrouturou. Comparaison of serval upwind scemes for multi-component one dimensional inviscid flows. *INRIA research report*, 1253, june 1990.
5. W. Fickett and W.C. Davis. Detonation. Technical report, University of California Press, Berkeley, 1979.
6. R. K. Fedkiw, T. Aslam, B. Merriman and S. Osher. A non oscillatory Eulerian approach to interfaces in multimaterials flows (the Ghost Fluid Method). *J. Comp. Phys.* **152**, pp. 457–492, 1999.
7. Fried E. CHEETAH 1.39 user's manual. UCRL-MA-117541 Rev 3, Energetic Material Center. Lawrence Livermore National Laboratory, 1996.
8. I.-L. Chern, J. Glimm, O. McBryan, B. Plohr, and S. Yaniv. Front tracking for gas dynamics, *J. Comput. Phys.*, **62**, pp. 83–110, 1986.
9. E. Godlewski and P.A. Raviart Numerical approximation of hyperbolic systems of conservation laws. Applied Mathematical Sciences. 118. New York, NY Springer. viii, 509 p.
10. S.K. Godunov A finite difference method for the numerical computation of discontinuous solutions of the equations of fluid dynamics *Mat. Sb.* **47** 357–393, 1959
11. S.K. Godunov, A. Zabrodine, M. Ivanov, A. Kraiko and G. Prokopov. Résolution numérique des problèmes multidimensionnels de la dynamique des gaz. Editions Mir, Moscow, 1979.
12. F. Hartlow and A. Amsden Fluid Dynamics, LANL monograph LA-4700 (1971)
13. J.-F. Hass and B. Sturtevant. Interaction of a weak shock waves with cylindrical and spherical gas inhomogeneities. *J. Fluid Mech.*, **181**, pp. 41–76, 1987.
14. S. Karni. Multi-component flow calculations by a consistent primitive algorithm. *J. Comp. Phys.*, **112**, pp. 31–43, 1996.
15. S. Karni. Hybrid multifluid algorithms. *SIAM J. Sci. Comput.* , **17**, no 5, pp. 1019–1039, 1996.
16. B. Larrouturou. How to preserve the mass fraction positivity when computing compressible multi-component flows. *J. Comput. Phys.*, **40**, no 2, pp. 263–293, 1981.
17. J. Massoni, R. Saurel, G. Baudin, and G. Demol A mechanistic model for shock initiation of solid explosives. *Physics of Fluids*, **11**, no 3, pp. 710–736, 1999.
18. P.A. Persson, R. Holmberg , and J. Lee Rock blasting and explosive engineering. Technical report, CRC Press, 1996.
19. P.L. Roe Riemann solvers, parameter vectors and difference schemes. *J. Comput. Phys.*, **43**, no. 2, pp. 357–372, 1981.
20. V. V. Rusanov. Calculation of interactions of non steady shock waves with obstacle. *J. Comput. Math. & Phys.* USSR **1**, pp. 267–279 (1961)

21. R. Saurel DPEX : Un outil numérique pour la détermination des cinétiques réactionnelles des explosifs fortement non idéaux. Technical report, Rapport de contrat Centre d'Etudes de Gramat - IUSTI, 1996.
22. R. Saurel, S. Mencacci, and S. Mercier HYDRO3D: Un outil simple pour la simulation de problèmes de détonique. EuroPyro 99, 7eme congrès international de pyrotechnie du GTPS, Brest 1999.
23. R. Saurel and R. Abgrall. A simple method for compressible multifluid flows. *Siam J. Sci. Comp.*, **21** , no 3, pp. 1115–1145, 1999.
24. R. Saurel and R. Abgrall. A multiphase Godunov method for compressible multifluid and multiphase flows. *J. Comput. Phys.*, **150**, no 2, pp. 425–467, 1999.
25. D. Serre Systems of conservation laws. I: Hyperbolicity, entropies, shock waves. Translated from the French by I. N. Sneddon. *Cambridge: Cambridge University Press. XXII, 263 p.* 1999.
26. K.M. Shyue An efficient shock capturing shock–capturing scheme for multicomponent problems. *J. Comput. Phys.* **142**, no 1, pp. 208–242, 1998.
27. E.F. Toro Some IVPs for which conservative methods fail miserably. in *Proceedings, 6th International Symposium on Computational Fluid Dynamics, Lake Tahoe, California,* September 4–8, 1995
28. E.F. Toro Riemann solvers and numerical methods for fluid dynamics. (Springer Verlag, Berlin, 1997).
29. Yee, H.C. Construction of explicit and implicit symmetric TVD schemes and their applications. *J. Comput. Phys.* 68, 151-179 (1987).

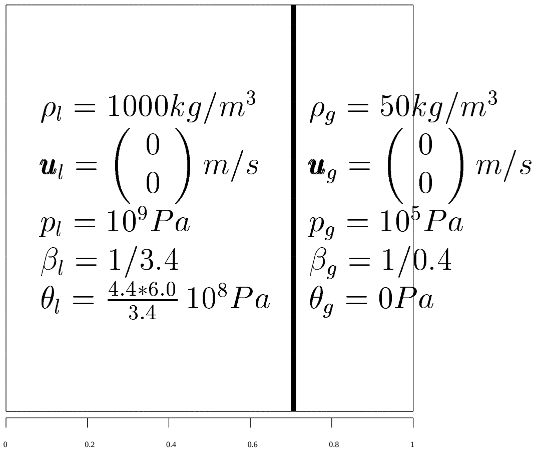

Figure 5. Initialization of the water-air shock tube: Test 1

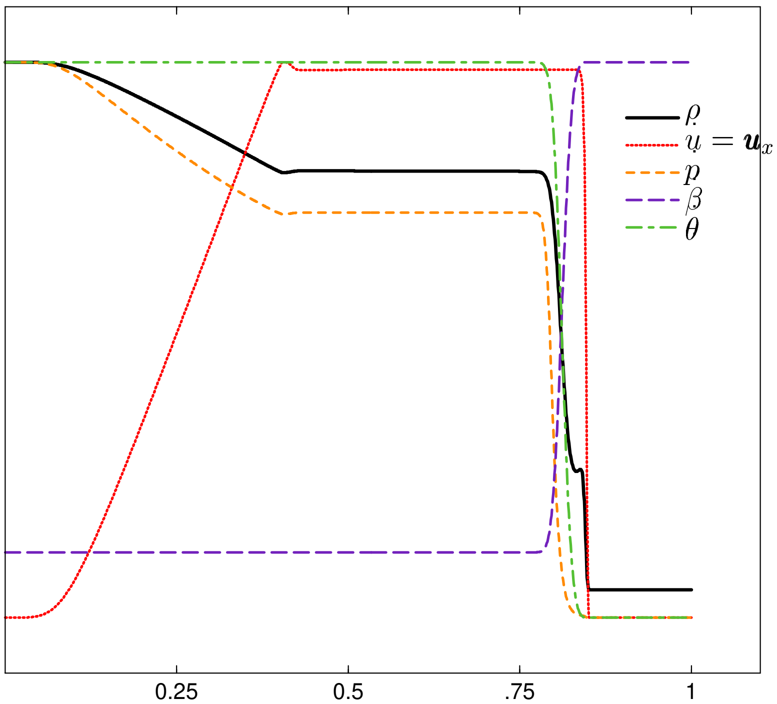

Figure 6. Density, velocity pressure and EOS parameters at the finial time $230\mu s$, Roe's flux and second order accurate MUSCL scheme on unstructured mesh.

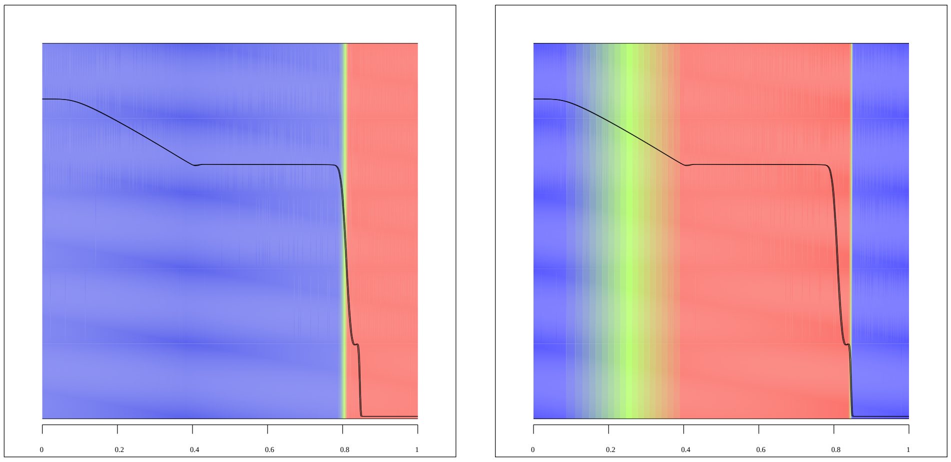

Figure 7. Iso-values of material parameter β (left) and velocity $\boldsymbol{u}_x$ (right) compared with the density profile on the boundary; Roe's flux and second order accurate MUSCL scheme on unstructured mesh.

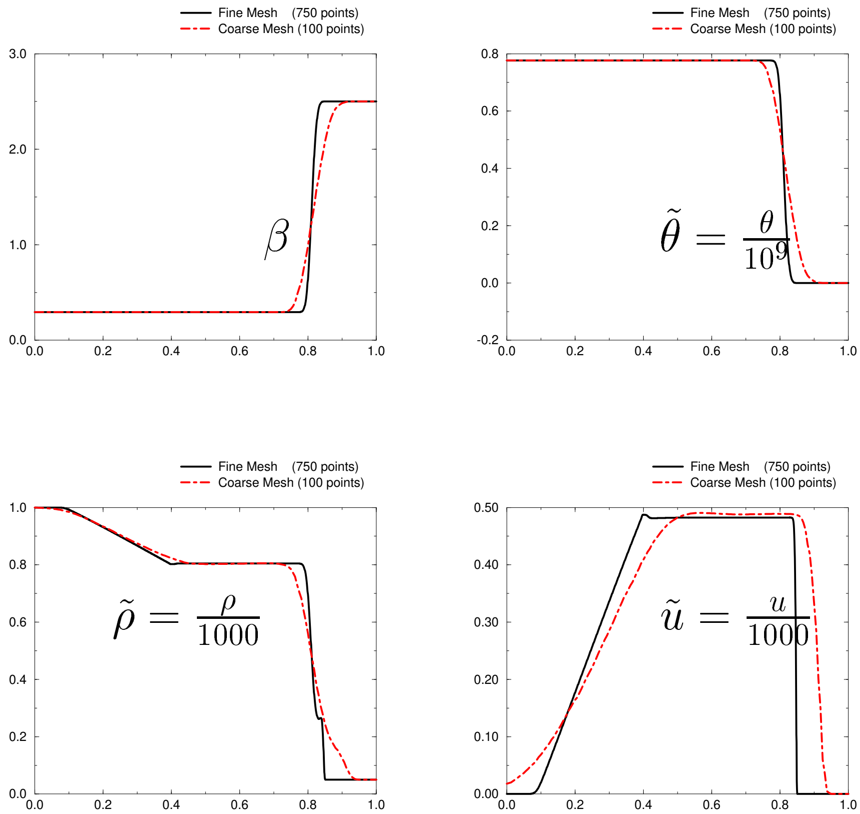

Figure 8. Comparison between the computations with the second order accurate MUSCL scheme for an unstructured coarse mesh of about 100 points in the propagation direction and an unstructured fine mesh of about 750 points in the propagation direction.

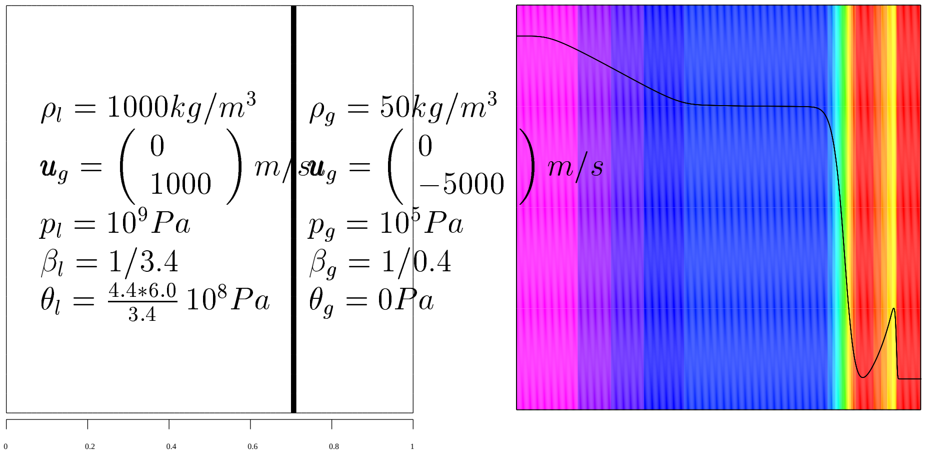

Figure 9. Initialization of the water-air shock tube, Test case 2 (left) and numerical solution with the Rusanov's flux, first order conservative scheme at the finial time $230\mu s$ (right): structured mesh of 705×3 nodes.

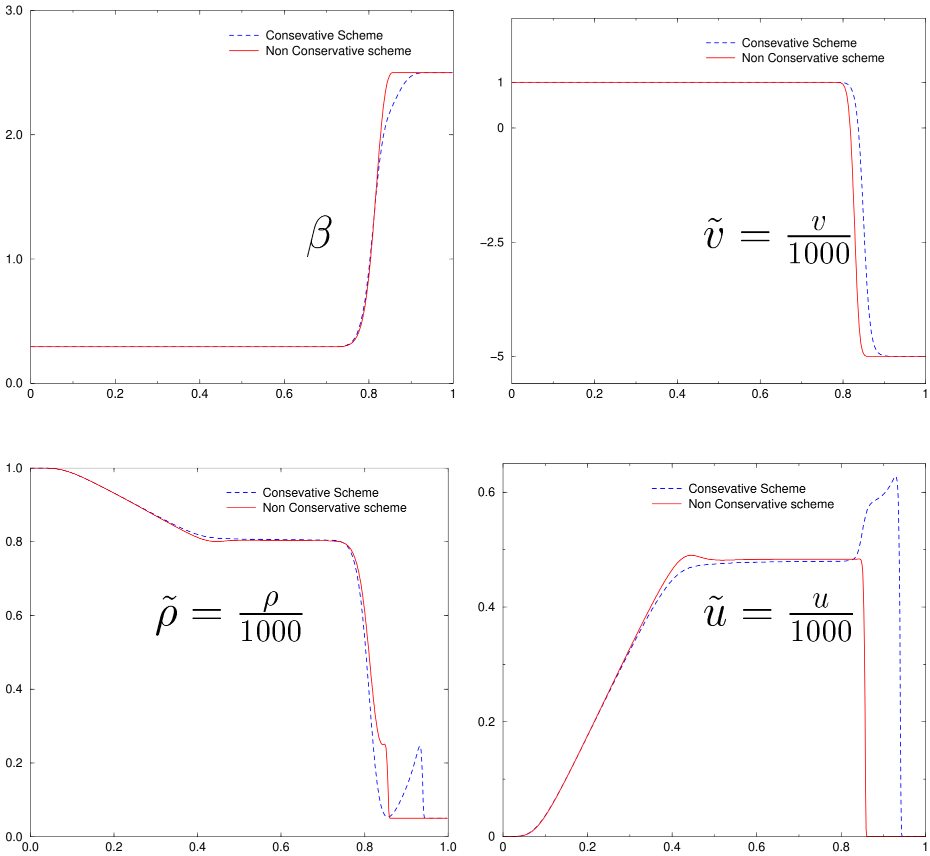

Figure 10. Comparison between the conservative and the non conservative scheme. Numerical solution with the Rusanov's flux, first order conservative scheme, at the finial time $230\mu s$: structured mesh of 705×3 nodes.

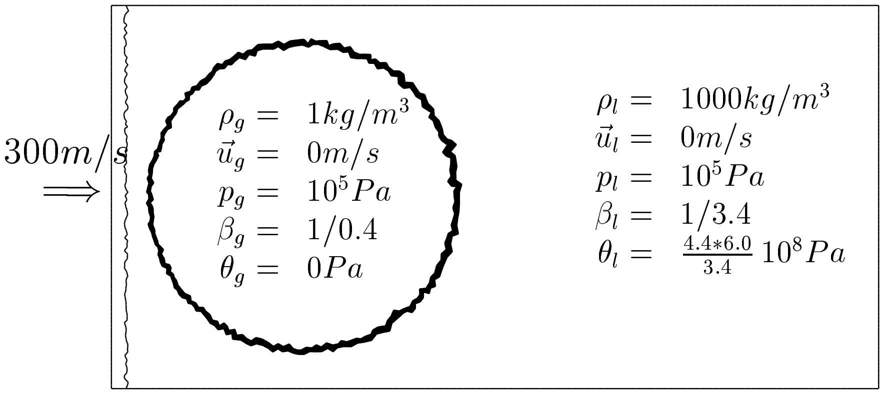

Figure 11. Initialization of the shock bubble interaction test case.

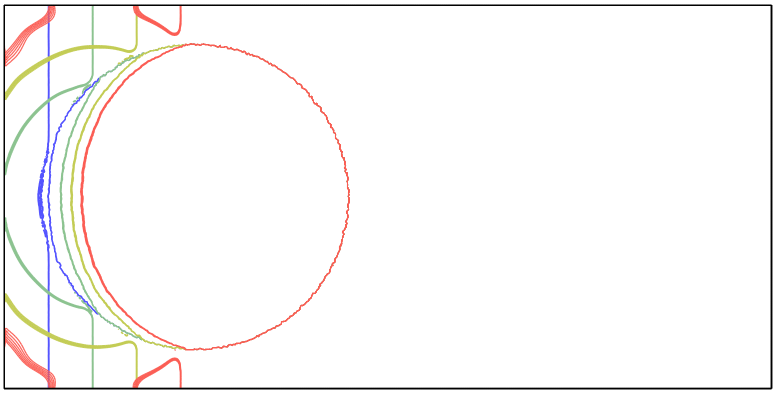

Figure 12. Evolution of the reflected, the refracted and the incident shock waves. Times $t = 0.65ms$, $t = 1.30ms$, $t = 1.95ms$ and $t = 2.6ms$.